
Thermodynamics and stability of a β -sheet complex: Molecular dynamics simulations on simplified off-lattice protein models

HYUNBUM JANG,¹ CAROL K. HALL,¹ AND YAOQI ZHOU²

¹Department of Chemical Engineering, North Carolina State University, Raleigh, North Carolina 27695-7905, USA

²Department of Physiology and Biophysics, State University of New York at Buffalo, Buffalo, New York 14214, USA

(RECEIVED April 25, 2003; FINAL REVISION September 3, 2003; ACCEPTED September 17, 2003)

Abstract

We have performed discontinuous molecular dynamics simulations of the thermodynamics and stability of a tetrameric β -sheet complex that contains four identical four-stranded antiparallel β -sheet peptides. The potential used in the simulation is a hybrid Go-type potential characterized by the bias gap parameter g , an artificial measure of the preference of a model protein for its native state, and the intermolecular contact parameter η , which measures the ratio of intermolecular to intramolecular native attractions. Despite the simplicity of the model, a complex set of thermodynamic transitions for the β -sheet complex is revealed that shows there are three distinct oligomer (partially ordered, ordered, and highly ordered β -sheet complex) states and four noninteracting monomers phases. The thermodynamic properties of the three oligomer states strongly depend on both the size of the intermolecular contact parameter η and the temperature. The partially ordered β -sheet complex is made up of four ordered globules and is observed at intermediate to large η at high temperatures. The ordered β -sheet complex contains four native β -sheets and is located at small to intermediate η at low temperatures in the phase diagram. The highly ordered β -sheet complex has fully-stiff β -sheet strands, the same as the global energy minimum structure, and is observed for all η at low temperatures.

Keywords: fibril; amyloid; discontinuous molecular dynamics; Go-type potential; β -sheet complex; bias gap; intermolecular contact parameter

Ordered protein aggregates are implicated in a number of so-called protein deposition diseases (Massry and Glasscock 1983; Eaton and Hofrichter 1990; Clark and Steele 1992; Gallo et al. 1996; Moore and Melton 1997). The best known of these diseases is Alzheimer's disease (Selkoe 1991; Simmons et al. 1994), which is characterized, on a molecular level, by the assembly of normally soluble proteins into insoluble fibril plaques in the extracellular space of brain tissue. The fibrils found in Alzheimer's disease victims are composed of β -sheets of the β -amyloid peptide ($A\beta$), whose monomeric form is a random coil or α -helix (Esler et al. 1996, 2000; Sunde et al. 1997; Benzinger et al.

1998, 2000; Burkoth et al. 1998; Lazo and Cowing 1998; Lynn and Meredith 2000; Zhang et al. 2000). Although amyloid fibrils commonly exhibit a cross- β structure, the exact nature of the β -sheet conformations in these aggregates is still ambiguous (Serpell 2000). Furthermore, the causes of amyloid fibril formation and the fundamental mechanisms underlying this type of aggregation are largely unknown.

The mechanism whereby isolated proteins change their conformations and assemble into an ordered oligomer is the subject of a number of recent investigations. The most popular view of protein aggregation is that partially unfolded states serve as precursors to fibril formation (Kelly 1996), because hydrophobic residues that are exposed to solution tend to cluster together. This view is supported by several recent experimental (Booth et al. 1997; Fink 1998; Guijarro et al. 1998; Chiti et al. 1999; Quintas et al. 1999;

Reprint requests to: Carol K. Hall, Department of Chemical Engineering, North Carolina State University, Raleigh, NC 27695-7905, USA; e-mail: hall@turbo.che.ncsu.edu; fax: (919) 515-3465.

Article and publication are at <http://www.proteinscience.org/cgi/doi/10.1110/ps.03162804>.

Khurana et al. 2001) and simulation (Harrison et al. 1999, 2001) studies of protein aggregation but is, by no means, universal. An alternative mechanism is indicated by the work of Silow et al. (1999), who have shown that ordered protein aggregates are formed directly from unfolded proteins in the two-state folders U1A and CI2; such behavior has also been observed in a recent simulations study of protein aggregation (Dima and Thirumalai 2002). Whether or not either mechanism explains amyloid formation in general is unclear; there may be a number of different mechanisms behind protein aggregation just as isolated proteins exhibit a number of distinct folding mechanisms on the molecular level.

The long-term goal of our work is to reveal the molecular-level mechanisms underlying protein aggregation and fibril formation, with particular focus on the role played by β -strands. Our approach is to use low-resolution or simplified protein models; such models are, in our opinion, best suited for simulating multiprotein systems because they allow us to study folding behavior over relatively long time-scales. Investigations based on these coarse-grained protein models by other investigators have already provided some insights into the thermodynamic and kinetic properties of protein folding for isolated chains (Lau and Dill 1989; Skolnick and Kolinski 1991; Miller et al. 1992; Chan and Dill 1994; Guo and Thirumalai 1995, 1996; Kolinski et al. 1995, 1999; Guo and Brooks III 1997; Gupta and Hall 1997; Zhou and Karplus, 1997a,b, 1999; Dokholyan et al. 1998, 2000; Nymeyer et al. 1998; Pande and Rokhsar 1998; Gupta et al. 1999; Shea et al. 2000; Jang et al. 2002a,b) and of protein aggregation for multichain systems (Dill and Stigter 1995; Gupta and Hall 1998; Harrison et al. 1999, 2001; Bratko and Blanch 2001; Dima and Thirumalai 2002; Jang et al. 2003). We recently introduced three minimalist models of four-strand antiparallel β -strand peptides: the β -sheet, the β -clip, and the β -twist (Jang et al. 2002a,b). In our study of the folding thermodynamics of these three models (Jang et al. 2002a), discontinuous molecular dynamics (DMD) simulations (Alder and Wainwright 1959; Rapaport 1978; Smith et al. 1996) were performed in order to determine how the thermodynamic properties of an isolated peptide vary with temperature. Despite the simplicity of these models, they undergo a complex set of protein transitions similar to those observed in experimental studies on real proteins (Ptitsyn 1995). Starting from high temperature, these transitions include a collapse transition, a disordered-to-ordered globule transition, a folding transition, and a liquid-to-solid transition. In our study of the folding kinetics for the same models (Jang et al. 2002b), the β -sheet exhibits a fast-track folding pathway without becoming trapped in any intermediate. In contrast, the β -clip and β -twist exhibit multiple folding pathways that include trapping in intermediates and direct folding to the native state. The folding speed of the model proteins with different native state topologies strongly de-

pends on the contact order in the native state (Plaxco et al. 1998).

In this article, we investigate the thermodynamics and stability of a tetrameric β -sheet complex, consisting of four identical four-stranded antiparallel β -sheet peptides (the β -sheet peptides studied previously), with each peptide containing 39 connected residues (beads). We have already investigated the kinetics and assembly of the β -sheet complex (Jang et al. 2003). In that study, four separate random coils were quenched from a high temperature to a low temperature, the temperature at which the peptides are in their β -sheet native state. After quenching, the four monomer chains experienced a conformational change toward the highly ordered β -sheet complex (folded state) or to a partially folded or disordered (misfolded) state. The formation kinetics and resulting structure at fixed temperature strongly depended upon the size of the intermolecular contact parameter η , which measures the ratio of intermolecular to intramolecular native attractions. For small η , most folding trajectories follow the following path: four monomers \rightarrow dimer and two monomers \rightarrow trimer and monomer or two dimers \rightarrow tetramer. The folding yield is low, and secondary structure begins to form before an ordered β -sheet complex assembles. For intermediate η , most folding trajectories follow the following path: four monomers \rightarrow dimer and two monomers \rightarrow trimer and monomer \rightarrow tetramer. The folding yield is very high, and four partially folded chains assemble into a highly ordered β -sheet complex. For large η , most folding trajectories follow the same path as seen in the intermediate η model. The folding yield is very low, and the four random coil monomers directly assemble into a highly ordered β -sheet complex. The results of the kinetics study for the β -sheet complex presented in our previous article set the stage for this work in which we examine the thermodynamics and stability of the β -sheet complex.

Our model of the β -sheet complex was designed in part to mimic the small A β oligomers that are observed (albeit indirectly) in the early stages of fibril formation (Harper et al. 1997). These oligomers are now widely believed to serve as the nuclei that seed the growth of the fibrils that characterize Alzheimer's and other amyloid diseases (Pallitto and Murphy 2001). In fact, recent evidence indicates that it is these oligomers, rather than the fully formed fibrils, that are the toxic species in Alzheimer's disease (Kirkitadze et al. 2002). Our model was designed in part to mimic real A β oligomer complex formation in several respects. First, our peptides are 39 residues long, and A β is between 39 and 42 residues long. Second, A β has several extended stretches of hydrophobic residues (A β [17–21], A β [32–42]); our peptide has essentially four stretches of residues that act with an intermolecular hydrophobic interaction. Third, the A β peptides in A β fibrils (and, indeed, the peptides in all fibrils) experience intramolecular hydrogen bonding within the

β -sheets and intermolecular hydrophobic interactions between the β -sheets. The model peptides in our β -sheet complex experience intramolecular interactions within the sheets that are reminiscent of hydrogen bonding; these interactions are characterized by the Go-model bias gap parameter, g . They also experience intermolecular interactions between the sheets that are reminiscent of hydrophobic interactions; these interactions are characterized by the intermolecular contact parameter η .

The Go-model bias gap parameter is set to an intermediate value ($g = 0.9$). Go models with intermediate values of the bias gap parameter are considered to be the most realistic compared with other values of the bias gap parameter, because all nonbonded pairs of beads are attracted to each other. The problems associated with large values of g are avoided (unfavorable repulsive forces between nonnative pairs of beads for $g > 1.0$ or no forces for $g = 1.0$), as are the problems associated with low values of g (near indistinguishability between native and nonnative interactions hinders the formation of the target native structure).

In our model, the intermolecular contact parameter η , which essentially measures the ratio of the intermolecular (hydrophobic) interaction and the intramolecular (hydrogen bonding) interaction, is selected in the range between $0.2 \leq \eta \leq 1$. The reasons for considering a range of intermolecular contact parameter values are as follows: (1) the best values for the relative strengths of the hydrophobic and hydrogen bonding interactions in simplified models are a matter of debate (Pace et al. 1998), and (2) intermolecular hydrophobic interaction strengths depend upon the intrinsic conditions of the protein (sequence and number of hydrophobic residues) and on external conditions (pH and temperature; Fraser et al. 1991a,b; Snyder et al. 1994; Kowalewski and Holtzman 1999). Furthermore, by exploring how the aggregation mechanism varies with the intermolecular contact parameter, we provide insights to other researchers interested in modeling aggregation phenomena.

In this article, we investigate the thermodynamic properties and stability of the tetrameric β -sheet complex, the same model as the one we investigated in the study of kinetics and assembly of the β -sheet complex (Jang et al. 2003). DMD simulations (Alder and Wainwright 1959; Rapaport 1978; Smith et al. 1996) were performed on the model systems at an intermediate value of the bias gap $g = 0.9$ for different intermolecular contact parameters in the range $0.2 \leq \eta \leq 10$ at different temperatures. All simulations were started from folded states of the complex; these configurations were obtained from our previous kinetic simulations. For each value of η and temperature, at least five independent simulations were performed to obtain equilibrium averages. The phase transitions of the β -sheet complex were determined by calculating thermodynamic averages for the fraction of native contacts Q , the squared

radius of gyration R_g^2 , the specific heat C_v , the internal energy E , the root-mean-squared pair separation fluctuation Δ_B , and the Lindemann disorder parameter Δ_L . The results are summarized in a phase diagram for the β -sheet complex in the temperature/intermolecular contact parameter η plane.

In the following section, a description of the model and the simulation method are presented. Next is the Results section, which is divided into four subsections: The first presents the results for the fraction of native contacts and the radius of gyration, the second presents the results for the specific heat and the internal energy, the third presents the results for the bead fluctuations, and the fourth presents the phase diagram for the β -sheet complex. The article concludes with a discussion of the key findings.

Models and simulation method

We consider an off-lattice protein model of a β -sheet complex that consists of four identical four-stranded antiparallel β -sheet peptides. The global energy minimum structure for the model β -sheet complex is shown in Figure 1. Each chain in the β -sheet complex is shaded differently: chain 1 (white), chain 2 (light gray), chain 3 (dark gray), and chain 4 (black). A topology diagram representing a top view of the complex is shown at the bottom of the figure. In the topology diagram, thick arrows indicate chain connectiv-

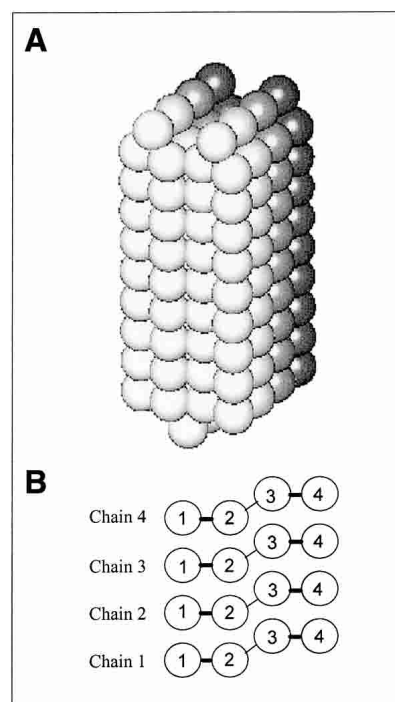


Figure 1. Bead (A) and topology (B) diagrams of the global energy minimum structures for the model β -sheet complex.

ity at the top of the strands, and thin arrows indicate chain connectivity at the bottom of the strands. It can be seen from the topology diagram that the β -sheet is not perfectly planar because it has an inflection in the middle. This is because β -sheet complex with kinked β -sheets has more intermolecular native contacts than that with planar β -sheets. In the global energy minimum state of the β -sheet complex, the total number of intramolecular native contacts is $N_{\text{intra}}^{\text{gem}} = 300$, the total number of intermolecular native contacts is $N_{\text{inter}}^{\text{gem}} = 522$, and the reduced squared radius of gyration for the entire system is $R_g^2 / \sigma^2 = 10.3495$.

The model β -sheet complex contains a total of 156 (M) beads, each representing an amino acid residue that can be regarded as being localized at the C_α atom. Each β -sheet monomer contains 39 (M_n) connected beads, so that $M = 4 \times M_n$. Nonbonded beads can interact with each other through a square-well or square-shoulder potential (Zhou et al. 1996, 1997). The details of the model potential are described in earlier publications (Jang et al. 2002a, 2003). For the β -sheet complex, however, the square-well depth or square-shoulder height, $B_{ij}\varepsilon$, used by the model potential is different from that for an isolated chain. The quantity $B_{ij}\varepsilon$ represents the interaction strength between nonbonded residue pair i and j and is defined as

$$B_{ij}\varepsilon = \begin{cases} B_N^{\text{intra}}\varepsilon, & \text{Intramolecular native contacts} \\ B_O\varepsilon, & \text{Non-native contacts} \\ B_N^{\text{inter}}\varepsilon, & \text{Intermolecular native contacts,} \end{cases} \quad (1)$$

where B_N^{intra} , B_O , and B_N^{inter} are measures of the relative strengths of the energies associated with the intramolecular native, nonnative, and intermolecular native pair interactions in this Go-type potential (Taketomi et al. 1975; Go and Taketomi 1978, 1979; Ueda et al. 1978). Within a chain, nonbonded pairs of beads that are in contact in the global energy minimum structure experience an attractive interaction, that is, $B_N^{\text{intra}} < 0$, when their square-wells overlap. On the other hand, within a chain and in different chains, nonbonded pairs of beads that are not in contact in the global energy minimum structure experience either an attractive interaction ($B_O < 0$) or a repulsive interaction ($B_O > 0$). The sign of the parameter B_O depends on the size of the bias gap parameter g ,

$$B_O = (1 - g)B_N^{\text{intra}}, \quad (B_N^{\text{intra}} < 0, g > 0), \quad (2)$$

where g is the bias gap (Zhou and Karplus 1997a,b, 1999; Jang et al. 2002a,b). The bias gap measures the ratio of the interaction strength between the intramolecular native contacts and nonnative contacts. Note that for $g < 1$, $B_O > 0$; in this case, nonnative contacts are repulsive so that the native state structure is strongly favored over any nonnative state structure. For $0 < g < 1$, $B_O < 0$, all nonbonded contact pairs

are attractive, but the intramolecular native contacts are always more favorable than are the nonnative contacts. For $g = 0$, the intramolecular native and nonnative contacts are equally favorable, $B_O = B_N^{\text{intra}}$, and the model reduces to a homopolymer. The bias gap is an artificial measure of the preference of a model protein for its native state; in a real protein, this preference for the native state might be measured, for example, by the energy difference between the native and nonnative state.

In different chains, bead pairs that are in contact in the global energy minimum structure experience an attractive interaction, that is, $B_N^{\text{inter}} < 0$, when their square-wells overlap. The parameter B_N^{inter} depends on the size of the intermolecular contact parameter η ,

$$B_N^{\text{inter}} = \eta B_N^{\text{intra}}, \quad (0 < \eta \leq 1), \quad (3)$$

where η is the intermolecular contact parameter (Jang et al. 2003). The quantity η measures the ratio of the interaction strength between the intermolecular and intramolecular native contacts. For $\eta = 1$, the intramolecular and intermolecular native contacts are equally favorable, that is, $B_N^{\text{inter}} = B_N^{\text{intra}}$. For $\eta < 1$, the intramolecular native contacts are more favorable than the intermolecular native contacts, that is, $B_N^{\text{inter}} > B_N^{\text{intra}}$. However, nonnative contacts are always less favorable than are the intramolecular and intermolecular native contacts, so that $B_N^{\text{intra}} \leq B_N^{\text{inter}} < B_O$ for $g > 0$. In this model, the intramolecular native interaction, intermolecular native interaction, and nonnative interaction might be regarded as mimicking hydrogen bonding, hydrophobic interactions, and van der Waals interactions, respectively, because in real fibrils, the molecular interactions along the sheets (generally hydrogen bonds) are different from the molecular interactions between the sheets (generally hydrophobic interactions).

The thermodynamic properties and stability of the β -sheet complex are investigated by using the DMD algorithm (Alder and Wainwright 1959; Rapaport 1978; Smith et al. 1996). All simulations were started from the folded state of the complex, which was obtained from our previous kinetic simulations on the same model (Jang et al. 2003). The initial configurations of the folded β -sheet complex were selected from different folding trajectories in the kinetic simulations to ensure that they are independent. All initial configurations of the folded β -sheet complexes were pre-equilibrated for 100,000 collisions at the temperature of interest, and then equilibrium simulations were performed. For simulations at low temperatures, the initial configurations were pre-equilibrated at a relatively high temperature, above the solid-to-liquid transition. This procedure was used to prevent the system from becoming trapped in a metastable or frozen state. Equilibrium simulations were performed for up to 4×10^8 collisions to ensure equilibra-

tion. For each value of η , at least five independent simulations at the temperature of interest were performed to obtain the equilibrium averages. Equilibrium averages were typically taken after discarding data from the first half of the simulation.

The progression of a conformational change was monitored by introducing the fraction of total native contacts formed (Sali et al. 1994; Lazaridis and Karplus 1997), Q_{total} , defined by

$$Q_{\text{total}} = \frac{\langle N_{\text{total}} \rangle_{\text{eq}}}{N_{\text{total}}^{\text{gem}}}, \quad (4)$$

where $\langle \rangle_{\text{eq}}$ denotes an average over the collisions after discarding the first half of the simulation, N_{total} is the total number of native contacts with $N_{\text{total}} \equiv N_{\text{intra}} + N_{\text{inter}}$, and $N_{\text{total}}^{\text{gem}}$ is the total number of native contacts in the global energy minimum state with $N_{\text{total}}^{\text{gem}} \equiv N_{\text{intra}}^{\text{gem}} + N_{\text{inter}}^{\text{gem}}$. The fraction of total native contacts is a weighted sum of the fraction of intramolecular native contacts, Q_{intra} , and the fraction of intermolecular native contacts, Q_{inter} ,

$$Q_{\text{total}} = (1 - \kappa)Q_{\text{intra}} + \kappa Q_{\text{inter}}, \quad (5)$$

where $Q_{\text{intra}} \equiv \langle N_{\text{intra}} \rangle_{\text{eq}} / N_{\text{intra}}^{\text{gem}}$, $Q_{\text{inter}} \equiv \langle N_{\text{inter}} \rangle_{\text{eq}} / N_{\text{inter}}^{\text{gem}}$, and κ is a constant, $\kappa = N_{\text{inter}}^{\text{gem}} / N_{\text{total}}^{\text{gem}} = 0.6350$. The degree of nativeness of the chains in the β -sheet complex was determined by measuring the fraction of intramolecular native contacts, Q_{intra} , whereas the dissociation of the β -sheet complex was monitored by examining the fraction of intermolecular native contacts, Q_{inter} , when $Q_{\text{inter}} = 0$.

To determine the locations of the thermodynamic transitions, the reduced specific heat and the reduced internal energy were determined. In calculating the specific heat and energy, the weighted histogram method (Ferrenberg and Swendsen 1989; Zhou et al. 1997) was used. Details of the method are reported elsewhere (Zhou et al. 1997). The squared radius of gyration for the entire system, R_g^2 , which monitors the dissociation of the system at high temperatures and the chain stiffness at low temperatures; the root-mean-squared (RMS) pair separation fluctuation, Δ_B , for the degree of bead mobility; and the Lindemann disorder parameter, Δ_L , for the low temperature transition were calculated. The details of the equations are described in earlier publications (Jang et al. 2002a, 2003).

Results

We performed DMD simulations to investigate the phase behavior of the β -sheet complex as a function of the size of the intermolecular contact parameter η and the reduced temperature, $T^* \equiv k_B T / \varepsilon$. Thermodynamic averages, including the fraction of native contacts Q , the squared radius of gy-

ration R_g^2 , the specific heat C_v , the internal energy E , the root-mean-squared pair separation fluctuation Δ_B , and the Lindemann disorder parameter Δ_L , were calculated as a function of temperature at intermolecular contact parameters, $\eta = 0.2, 0.3, 0.4, 0.5, 0.6, 0.7, 0.8, 0.9$, and 1.0 . The major results presented in this paper are for three selected values of the intermolecular contact parameters, $\eta = 0.2, 0.5$, and 0.8 .

Fraction of native contacts and radius of gyration

The fraction of total native contacts, $\langle Q_{\text{total}} \rangle$, the fraction of intramolecular native contacts, $\langle Q_{\text{intra}} \rangle$, and the fraction of intermolecular native contacts, $\langle Q_{\text{inter}} \rangle$, are shown in Figure 2 as a function of the reduced temperature, T^* , for the three selected intermolecular contact parameters: (1) $\eta = 0.2$, (2) $\eta = 0.5$, and (3) $\eta = 0.8$. Here, $\langle \rangle$ denotes the average over at least five independent simulations. The error bars are the standard deviation in the measured values and are only shown for values larger than the size of the symbol. The nativeness of the individual chains in the β -sheet complex can be measured by the fraction of intramolecular native contacts, $\langle Q_{\text{intra}} \rangle$. The dissociation of the complex can be identified by examining the fraction of intermolecular native contacts, $\langle Q_{\text{inter}} \rangle$.

In Figure 2A, for $\eta = 0.2$ the $\langle Q_{\text{intra}} \rangle$ values continuously decrease as T^* increases, whereas the $\langle Q_{\text{inter}} \rangle$ values decrease in steps at certain temperatures. The trend in the $\langle Q_{\text{total}} \rangle$ curve is a reflection of the trends in $\langle Q_{\text{intra}} \rangle$ and $\langle Q_{\text{inter}} \rangle$, because $\langle Q_{\text{total}} \rangle = (1 - \kappa)\langle Q_{\text{intra}} \rangle + \kappa\langle Q_{\text{inter}} \rangle$, where $\kappa = 0.6350$ as shown in equation 7. At $T^* = 0.09$, the discontinuity in the $\langle Q_{\text{inter}} \rangle$ curve corresponds to a solid-to-liquid transition, and at $T^* = 0.29$ the discontinuity corresponds to the system dissociation transition. At temperatures below $T^* = 0.09$, the β -sheet complex is in a solid-like phase with a highly ordered structure (see below); we will refer to this as the highly ordered β -sheet complex. The highly ordered β -sheet complex has large values of $\langle Q_{\text{intra}} \rangle$ and $\langle Q_{\text{inter}} \rangle$ with $\langle Q_{\text{intra}} \rangle \approx \langle Q_{\text{inter}} \rangle \approx 1$, indicating that its structure is similar to the global energy minimum structure shown in Figure 1. At temperatures between $T^* = 0.09$ and $T^* = 0.29$, the β -sheet complex is in an ordered state; we will refer to this as the ordered β -sheet complex. The ordered β -sheet complex has a large value of $\langle Q_{\text{intra}} \rangle$ with $\langle Q_{\text{intra}} \rangle > 0.95$, indicating that each chain in the ordered β -sheet complex is in its native state. However, its $\langle Q_{\text{inter}} \rangle$ value is smaller than that in the highly ordered β -sheet complex, indicating that the ordered β -sheet complex is loosely packed. At $T^* \geq 0.29$, the ordered β -sheet complex is completely separated into four monomers with $\langle Q_{\text{inter}} \rangle = 0$. The process of system dissociation starts at temperature $T^* = 0.27$ and ends at $T^* = 0.29$. During this transition process, various types of thermodynamic intermediates are observed. The structures of these intermediates

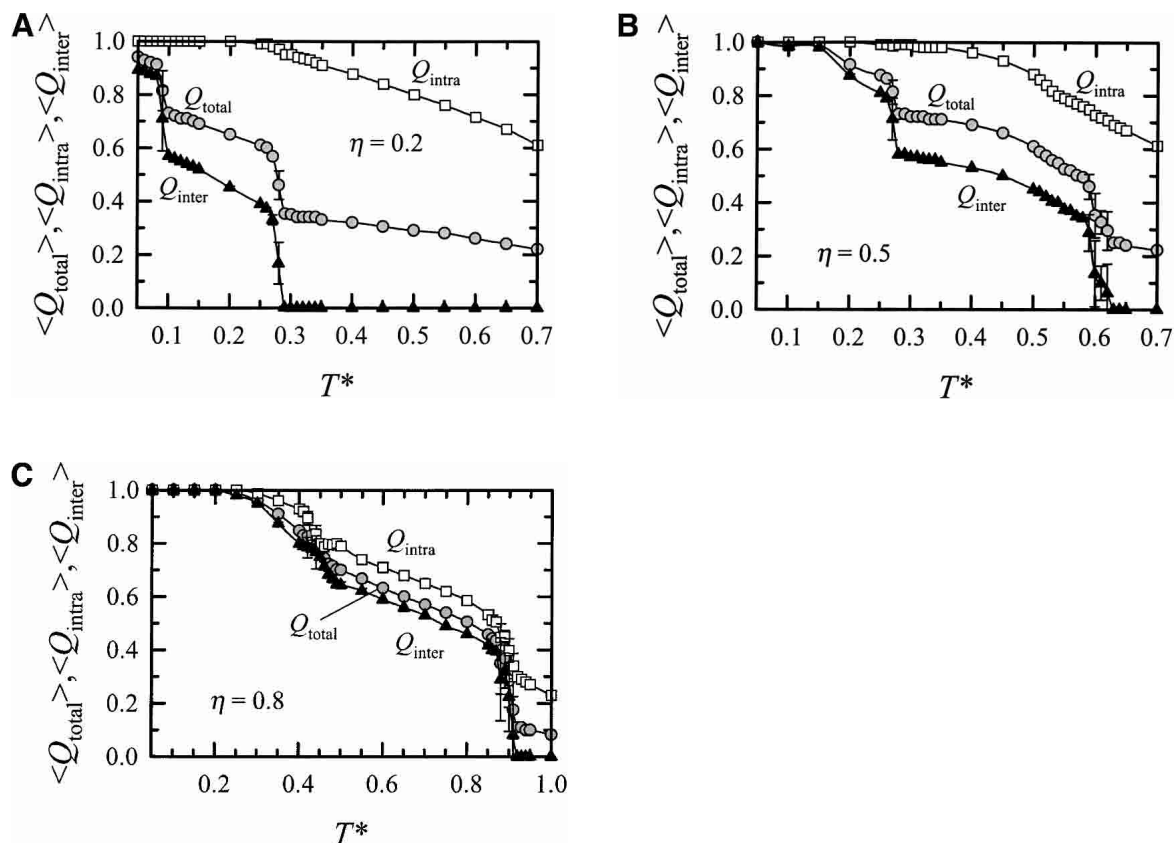


Figure 2. Average values of the fraction of total native contacts, $\langle Q_{total} \rangle$, the fraction of intramolecular native contacts, $\langle Q_{intra} \rangle$, and the fraction of intermolecular native contacts, $\langle Q_{inter} \rangle$, as a function of the reduced temperature, T^* , for three selected values of the intermolecular contact parameter η : $\eta = 0.2$ (A), $\eta = 0.5$ (B), and $\eta = 0.8$ (C).

are the same as the kinetic intermediates, I_{2+1+1} , I_{2+2} , and I_{3+1} that were observed in the kinetic simulations for the same model (Jang et al. 2003). The thermodynamic intermediates are only observed in the very narrow range of temperature, $0.27 < T^* < 0.29$, whereas the kinetic intermediates are observed at any temperature during the oligomerization in kinetic simulations. The four separated chains at $T^* = 0.29$ are each in the native state, that is, the native β -sheet. As T^* increases, each chain undergoes the folding transition at $T^* = 0.40$, the disordered-to-ordered globule transition at $T^* = 0.80$, and the collapse transition at $T^* = 0.95$ as seen in our thermodynamic study of the isolated β -sheet chain systems (Jang et al. 2002a).

For $\eta = 0.5$, the solid-to-liquid transition is observed at $T^* = 0.27$ and the system dissociation transition is located at $T^* = 0.60$, as indicated by the discontinuities in the $\langle Q_{inter} \rangle$ curve of Figure 2B. Both of the transition temperatures at $\eta = 0.5$ are higher than those observed at $\eta = 0.2$. At $T^* < 0.27$, the oligomer is the highly ordered β -sheet complex, which, as indicated earlier, is a solid-like phase. At much lower temperatures, $T^* \leq 0.15$, for the highly ordered β -sheet complex, $\langle Q_{total} \rangle \approx 1$, indicating that the highly ordered β -sheet complex is the same as the global

energy minimum structure shown in Figure 1. At $0.27 < T^* < 0.52$, the oligomer is the ordered β -sheet complex, which has the same physical properties as those observed at $\eta = 0.2$. The ordered β -sheet complex consists of four native β -sheets with large $\langle Q_{intra} \rangle$ values and is loosely packed with smaller $\langle Q_{inter} \rangle$ values than the highly ordered β -sheet complex. The ordered β -sheet complex remains intact with the β -sheets remaining in their native state at temperatures above the folding transition for the isolated β -sheets, $T^* = 0.40$ (Jang et al. 2002a). This indicates that the presence of the strong intermolecular native interactions stabilizes the ordered β -sheet complex structures at high temperatures. At $0.52 < T^* < 0.58$, the β -sheet complex is in a partially ordered state; we will refer to this as the partially ordered β -sheet complex. In fact, the transition at $T^* = 0.52$, between the ordered and the partially ordered β -sheet complexes is determined by a peak in the specific heat (see below). The partially ordered β -sheet complex is characterized by $\langle Q_{intra} \rangle$ values with $0.6 < \langle Q_{intra} \rangle < 0.85$; these are significantly smaller than the $\langle Q_{intra} \rangle$ values in the ordered β -sheet complex where $\langle Q_{intra} \rangle > 0.85$. This indicates that each chain in the partially ordered β -sheet complex is not in its native state but is instead in an ordered

globule state, a thermodynamic intermediate that is known as a molten globule (Ptitsyn 1995). The ordered globule state for $g = 0.9$ has Q values typically in the range $0.5 < Q < 0.9$ (Jang et al. 2002a). The partially ordered β -sheet complex, which consists of four ordered globules, is more loosely assembled than the ordered β -sheet complex, and consists of four native β -sheets, because it has smaller $\langle Q_{\text{inter}} \rangle$ values than the ordered β -sheet complex. The partially ordered β -sheet complex was not observed at $\eta = 0.2$. At $T^* = 0.58$, the partially ordered β -sheet complex starts to dissociate and is completely separated into four chains at $T^* = 0.63$ with $\langle Q_{\text{inter}} \rangle = 0$. A number of thermodynamic intermediates are observed during this dissociation process. The four separated chains at $T^* = 0.63$ are each in the ordered globule state. As T^* increases, each chain undergoes the ordered-to-disordered globule transition at $T^* = 0.80$ and the collapse transition at $T^* = 0.95$ as seen in our thermodynamic study of the isolated β -sheet chain systems (Jang et al. 2002a).

For $\eta = 0.8$ in Figure 2C, the solid-to-liquid transition is observed at $T^* = 0.44$, and the system dissociation transition is found at $T^* = 0.90$ as indicated by the discontinuities observed in the $\langle Q_{\text{inter}} \rangle$ curve. These transition temperatures are higher than those at $\eta = 0.5$, indicating that as η increases, both transitions are shifted to higher temperatures. At $T^* < 0.44$, the system is in the highly ordered β -sheet complex, a solid-like phase. At even lower temperature, $T^* \leq 0.25$, the highly ordered β -sheet complex with $\langle Q_{\text{total}} \rangle \approx 1$ is the same as the global energy minimum structure. At $0.44 < T^* < 0.87$, the system is the partially ordered β -sheet complex because it has $\langle Q_{\text{intra}} \rangle$ values in the range $0.5 < \langle Q_{\text{intra}} \rangle < 0.8$. The physical properties of the partially ordered β -sheet complex for $\eta = 0.8$ are the same as those observed at $\eta = 0.5$; that is, the partially ordered β -sheet complex consists of four loosely aligned ordered globules. No ordered β -sheet complex is observed for $\eta = 0.8$. The partially ordered β -sheet complex remains intact with the four ordered globules at temperatures above the ordered-to-disordered globule transition for the isolated β -sheets, $T^* = 0.80$. This indicates that the chains are more stable in the complex conformation than when they are isolated. At $T^* = 0.87$, the system starts to dissociate and is completely separated into four chains with $\langle Q_{\text{inter}} \rangle = 0$ by $T^* = 0.92$. Various types of thermodynamic intermediates are observed during the system dissociation process. The four separated disordered globules at $T^* = 0.92$ undergo a collapse transition toward the random coil state at $T^* = 0.95$ as seen in our thermodynamic study of the isolated β -sheet chain systems (Jang et al. 2002a).

The system size changes dramatically as the system separates into four monomers. This is reflected in the change in the reduced squared radius of gyration for the entire system, $\langle R_g^2/\sigma^2 M \rangle$, as a function of the reduced temperature, T^* , as shown in Figure 3. Here, \diamond denotes the average over at least

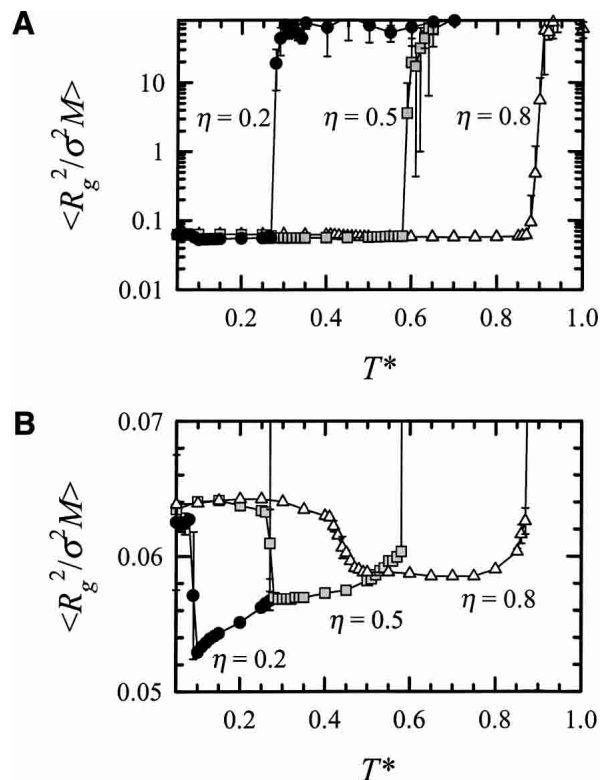


Figure 3. (A) Average values of the reduced squared radius of gyration per bead, $\langle R_g^2/\sigma^2 M \rangle$, on a logarithmic scale for three selected values of the intermolecular contact parameter, $\eta = 0.2, 0.5$, and 0.8 , as a function of the reduced temperature, T^* . (B) The same plot, but only showing behavior at low values of $\langle R_g^2/\sigma^2 M \rangle$.

five independent simulations. In Figure 3A, as T^* increases the $\langle R_g^2/\sigma^2 M \rangle$ values increase rapidly as a function of temperature at $T^* = 0.27, 0.58$, and 0.87 for $\eta = 0.2, 0.5$, and 0.8 , respectively, signaling the chain separation. These temperatures are consistent with the starting points of the system dissociation process at each η shown in Figure 2. In Figure 3, B is the same as A, but shows only the behavior at low values of $\langle R_g^2/\sigma^2 M \rangle$. It is immediately apparent that as T^* decreases, the $\langle R_g^2/\sigma^2 M \rangle$ values of the complex increase slightly at $T^* = 0.09, 0.27$, and 0.45 for $\eta = 0.2, 0.5$, and 0.8 , respectively, and then remain steady at even lower temperatures. The increase in the $\langle R_g^2/\sigma^2 M \rangle$ values at low temperature is related to the liquid-to-solid transition and is consistent with the low temperature discontinuity in the $\langle Q_{\text{inter}} \rangle$ values in Figure 2. At this transition, the ordered β -sheet complex at $\eta = 0.2$ and 0.5 and the partially ordered β -sheet complex at $\eta = 0.8$ turn into the highly ordered β -sheet complex by elongating their β -strands. The size of the system increases at this transition as the $\langle R_g^2/\sigma^2 M \rangle$ values increase at low temperature. The sizes of the ordered and the partially ordered β -sheet complexes are smaller than that of the highly ordered β -sheet complex as indicated by the depth of the “well” in the $\langle R_g^2/\sigma^2 M \rangle$ curves.

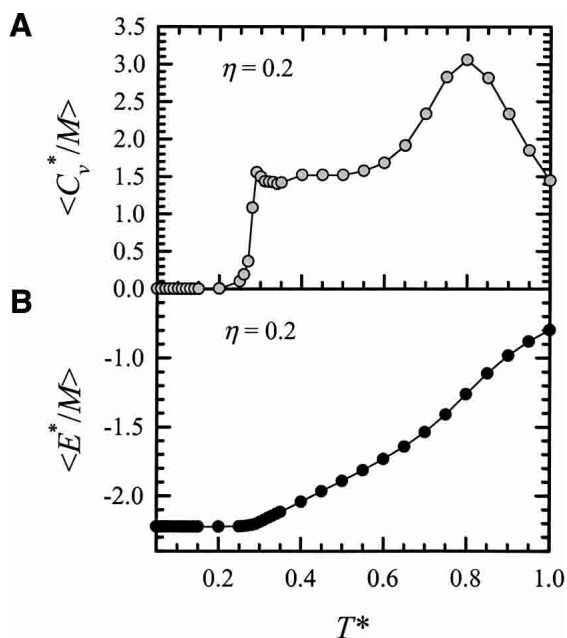


Figure 4. Average values of the reduced specific heat per bead, $\langle C_v^*/M \rangle$ (A), and the reduced internal energy per bead, $\langle E^*/M \rangle$ (B), for $\eta = 0.2$ as a function of the reduced temperature, T^* .

This indicates that the highly ordered β -sheet complex has highly stiff β -sheet strands, recovering the long molecular shape which increases the $\langle R_g^2/\sigma^2 M \rangle$ values. The size of the highly ordered β -sheet complex at very low temperatures is relatively independent of η and is very close to that of the global energy minimum structure.

Specific heat and energy

It is interesting to more precisely locate the thermodynamic transitions experienced by the β -sheet complex. For $\eta = 0.2$, Figure 4 shows (1) the reduced specific heat per bead, $\langle C_v^*/M \rangle$, and (2) the reduced internal energy per bead, $\langle E^*/M \rangle$, as a function of the reduced temperature, T^* . Here, $\langle \rangle$ denotes the average over at least five independent simulations. The results for the specific heat and the energy were obtained using the same weighted histogram method (Ferrenberg and Swendsen 1989) that was introduced in the study of homopolymers (Zhou et al. 1997). The equilibrium transition temperatures of the model can be identified from the peaks in the specific heat. In Figure 4A, the system dissociation transition for $\eta = 0.2$ can be identified by the peak at $T^* = 0.29$ in the specific heat curve. This is in good agreement with our observations that at $T^* = 0.29$, $\langle Q_{\text{inter}} \rangle = 0$ in Figure 2A and $\langle R_g^2/\sigma^2 M \rangle$ increases abruptly in Figure 3A. Below the transition, the system is in the ordered β -sheet complex state at low temperatures and in the highly ordered β -sheet complex state at even lower temperatures. No peak associated with the transition from the

ordered to the highly ordered β -sheet complex is observed in the specific heat. In fact, at this low value of the intermolecular contact parameter, $\eta = 0.2$, the contribution to the system energy from the intermolecular native interactions is very small. Above the system dissociation transition, the system separates into four native β -sheets. The weak plateau at $T^* = 0.40$ in the specific heat is associated with the folding transition for each separated chain. The peak at $T^* = 0.80$ in the specific heat is associated with the ordered-to-disordered transition for each separated chain. No peak or plateau associated with the collapse transition at $T^* = 0.95$ in the specific heat was observed for the monomers (Jang et al. 2002a). The high value for the specific heat in the monomer state is due to the large contribution to the energy arising from the intramolecular interactions of the individual β -sheets. In Figure 4B, the energy of the system remains the same in the highly ordered β -sheet complex at $T^* < 0.09$ and the ordered β -sheet complex at $0.09 < T^* < 0.29$, but increases monotonically with temperature after the system dissociates.

In Figure 5A, for $\eta = 0.5$ three distinct peaks in the specific heat are found at temperatures of $T^* = 0.27$, 0.52, and 0.60, which correspond to the solid-to-liquid, the ordered-to-partially ordered β -sheet complex, and the system dissociation transitions, respectively. The ordered-to-partially ordered β -sheet complex transition at $T^* = 0.52$ for $\eta = 0.5$ was not observed in the $\eta = 0.2$ model, because no partially ordered β -sheet complex was found. The small size of the peak in this transition indicates that there are no major changes in the structure as a whole, but the system

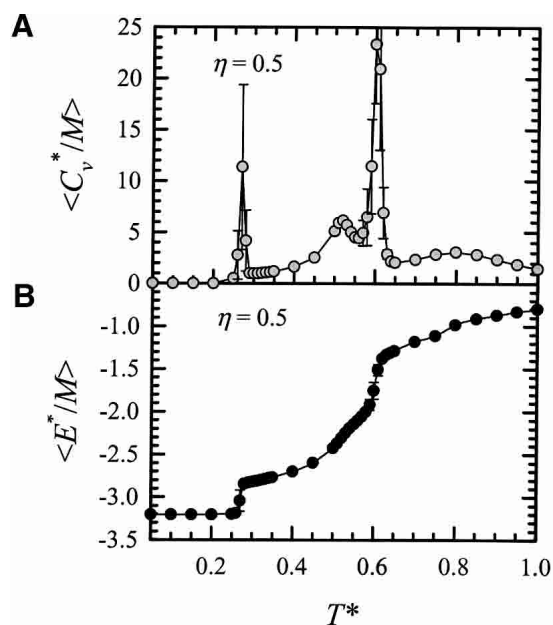


Figure 5. Average values of the reduced specific heat per bead, $\langle C_v^*/M \rangle$ (A), and the reduced internal energy per bead, $\langle E^*/M \rangle$ (B), for $\eta = 0.5$ as a function of the reduced temperature, T^* .

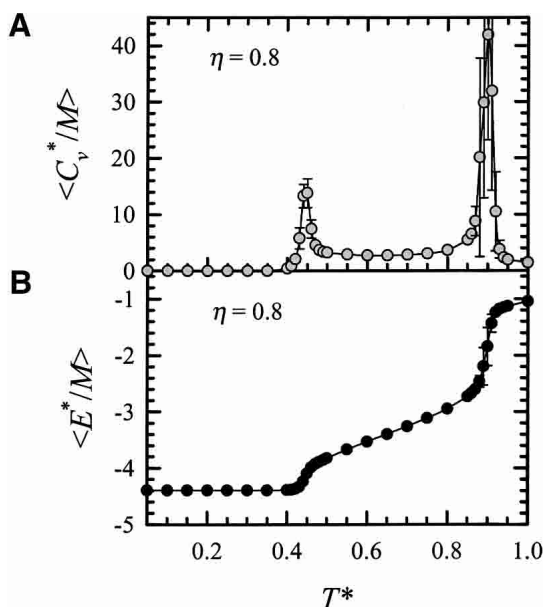


Figure 6. Average values of the reduced specific heat per bead, $\langle C_v^*/M \rangle$ (A), and the reduced internal energy per bead, $\langle E^*/M \rangle$ (B), for $\eta = 0.8$ as a function of the reduced temperature, T^* .

instead experiences a subtle conformational change. In fact, at this transition the energy change of the system is mainly due to a change in the conformation of the monomers from the ordered globule to the native state; that is, the energy change is due to the folding transition in the monomer state. Large energy changes of the system occur at both the solid-to-liquid transition at $T^* = 0.27$ and the system dissociation transition at $T^* = 0.60$. This is reflected in the two kinks in the $\langle E^*/M \rangle$ versus T^* curve at $T^* = 0.27$ and 0.60 in Figure 5B. Above the system dissociation transition, the system separates into four ordered globules. The broad plateau at $T^* = 0.80$ in the specific heat is associated with the ordered-to-disordered transition for each separated chain (Jang et al. 2002a).

For $\eta = 0.8$, two distinct peaks in the specific heat are observed in Figure 6A at $T^* = 0.45$ and 0.90 , which are related to the solid-to-liquid and the system dissociation transitions, respectively. Unlike the $\eta = 0.2$ and 0.5 models, the solid-to-liquid transition for $\eta = 0.8$ separates the highly ordered and the partially ordered β -sheet complexes. As mentioned above, no ordered β -sheet complex structure was observed in the $\eta = 0.8$ model. At $T^* = 0.45$, the partially ordered β -sheet complex has a conformational change toward the highly ordered β -sheet complex in which its β -strands elongate. At $T^* = 0.90$, the partially ordered β -sheet complex dissociates into four noninteracting disordered globules. Large energy changes associated with both transitions are reflected in the two kinks in the $\langle E^*/M \rangle$ versus T^* curve at $T^* = 0.45$ and 0.90 in Figure 6B.

Bead fluctuations

To determine the degree of bead mobility and to characterize the phase of the β -sheet complex, the RMS pair separation fluctuation, Δ_B , and the Lindemann disorder parameter, Δ_L , are calculated. For $\eta = 0.2$, Figure 7 shows (1) the RMS pair separation fluctuation, $\langle \Delta_B \rangle$, and (2) the Lindemann disorder parameter, $\langle \Delta_L \rangle$, on a logarithmic scale as a function of the reduced temperature T^* . In Figure 7A, a peak is observed at $T^* = 0.28$, indicating the system dissociation transition. The location of the peak is consistent with the fact that $\langle Q_{\text{inter}} \rangle = 0$ at $T^* = 0.29$ in Figure 2A, that $\langle R_g^2/\sigma^2 M \rangle$ increases abruptly at $T^* = 0.27$ as shown in Figure 3A, and that the specific heat has a peak at $T^* = 0.29$ in Figure 4A. The solid-to-liquid transition observed at low temperatures can be characterized by calculating the Lindemann disorder parameter (Lindemann 1910), as shown in Figure 7B. This parameter is often used to analyze the solid-to-liquid transition (Bilgram 1987; Löwen 1994; Stillinger 1995; Zhou et al. 1999). A form of the Lindemann criterion for melting is adopted here in which systems with $\Delta_L < 0.15$ are considered solid-like, whereas systems with $\Delta_L > 0.15$ are considered liquid-like. The dotted line in Figure 7B indicates the criterion for the melting transition. The solid-to-liquid transition obtained from the intersection between the $\langle \Delta_L \rangle$ curve and the dotted line in Figure 7B occurs at $T^* = 0.09$. This indicates that the highly ordered β -sheet complex at $T^* < 0.09$ is solid-like with $\Delta_{Li} < 0.15$, but the ordered β -sheet complex at $T^* > 0.09$ is liquid-like with $\Delta_{Li} > 0.15$. The location of the

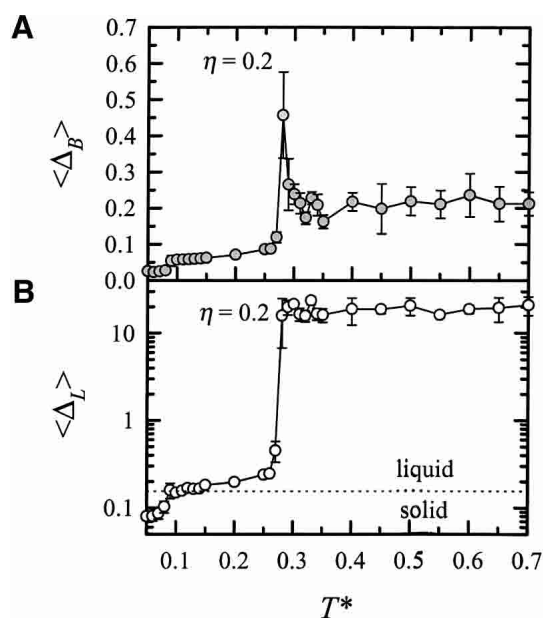


Figure 7. Average values of the root-mean-squared pair separation fluctuation, $\langle \Delta_B \rangle$ (A), and the Lindemann disorder parameter, $\langle \Delta_L \rangle$ (B), for $\eta = 0.2$ as a function of the reduced temperature, T^* .

solid-to-liquid transition obtained from Figure 7B is consistent with that of the low temperature discontinuities in the $\langle Q_{\text{inter}} \rangle$ curve in Figure 2A and in the $\langle R_g^2/\sigma^2M \rangle$ curve in Figure 3B.

For $\eta = 0.5$, Figure 8 shows (1) the RMS pair separation fluctuation, $\langle \Delta_B \rangle$, and (2) the Lindemann disorder parameter, $\langle \Delta_L \rangle$, on a logarithmic scale as a function of the reduced temperature T^* . In Figure 8A, a well-defined peak at $T^* = 0.61$ in the $\langle \Delta_B \rangle$ curve signals the system dissociation transition and is consistent with the peak at $T^* = 0.60$ in the specific heat curve in Figure 5A. In Figure 8B, the intersection between the $\langle \Delta_L \rangle$ curve and the dotted line that characterizes the solid-to-liquid transition is found at $T^* = 0.27$, which is consistent with the specific heat peak at $T^* = 0.27$ observed in Figure 5A.

For $\eta = 0.8$, Figure 9 shows (1) the RMS pair separation fluctuation, $\langle \Delta_B \rangle$, and (2) the Lindemann disorder parameter, $\langle \Delta_L \rangle$, on a logarithmic scale as a function of the reduced temperature T^* . In Figure 8A, a well-defined peak at $T^* = 0.90$ in the $\langle \Delta_B \rangle$ marks the system dissociation transition and is consistent with the peak found at $T^* = 0.90$ in the specific heat curve in Figure 6A. In Figure 8B, the intersection between the $\langle \Delta_L \rangle$ curve and the dotted line is found at $T^* = 0.43$, which is almost at the same location as the specific heat peak at $T^* = 0.45$ in Figure 6A. This peak characterizes the solid-to-liquid transition.

Snapshots and phase diagram

It is interesting to examine the structures of the β -sheet complex in the different thermodynamic phases. Snapshots

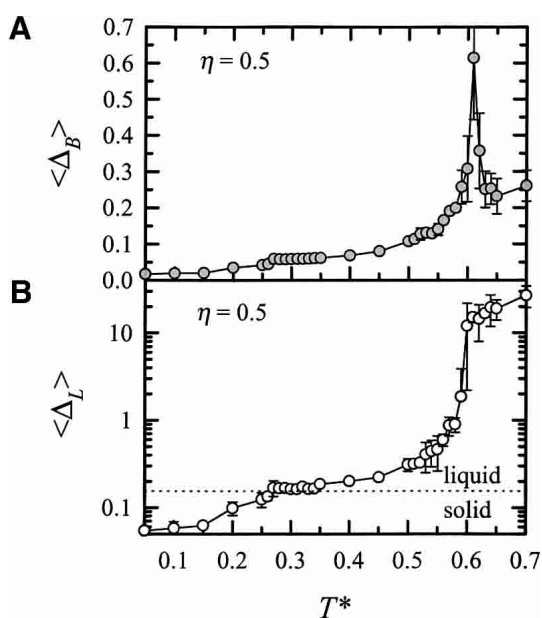


Figure 8. Average values of the root-mean-squared pair separation fluctuation, $\langle \Delta_B \rangle$ (A), and the Lindemann disorder parameter, $\langle \Delta_L \rangle$ (B), for $\eta = 0.5$ as a function of the reduced temperature, T^* .

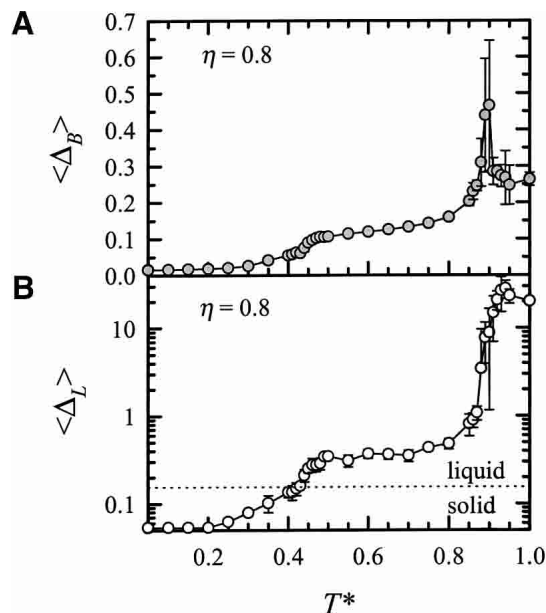


Figure 9. Average values of the root-mean-squared (rms) pair separation fluctuation, $\langle \Delta_B \rangle$ (A), and the Lindemann disorder parameter, $\langle \Delta_L \rangle$ (B), for $\eta = 0.8$ as a function of the reduced temperature, T^* .

representing typical structures observed for the β -sheet complex in the final state are presented in Figure 10 for (1) the partially ordered β -sheet complex, (2) the ordered β -sheet complex, and (3) the highly ordered β -sheet complex. The chains are shaded differently to enable the reader to distinguish one from the other. In Figure 10A, snapshots corresponding to the partially ordered β -sheet complex are shown for $\eta = 0.5$ at $T^* = 0.55$ and $\eta = 0.8$ at $T^* = 0.85$. It can be seen from Figure 10A that four native-like β -sheets are more or less aligned in parallel facing each other. The native-like β -sheets in the complex are the ordered globules, because the partially ordered β -sheet complex has $\langle Q_{\text{intra}} \rangle$ values in the range of $0.5 < \langle Q_{\text{intra}} \rangle < 0.9$. The partially ordered β -sheet complex is liquid-like, is loosely packed, and has large fluctuations in the bead motion. For $\eta = 0.2$, no partially ordered β -sheet complex is observed at any temperature we investigated. In Figure 10B, snapshots of the ordered β -sheet complex are shown for $\eta = 0.2$ at $T^* = 0.25$ and for $\eta = 0.5$ at $T^* = 0.33$. The ordered β -sheet complex contains four native β -sheets, which are well aligned in parallel facing each other. The ordered β -sheet complex is in a liquid-like phase, is loosely packed, and has smaller fluctuations in the bead motion than the partially ordered β -sheet complex; it is not observed in the $\eta = 0.8$ model at any of the temperatures we investigated. In Figure 10C, snapshots for the highly ordered β -sheet complex are shown for $\eta = 0.2$ at $T^* = 0.07$ and $\eta = 0.8$ at $T^* = 0.30$. The highly ordered β -sheet complex has large $\langle Q_{\text{intra}} \rangle$ and $\langle Q_{\text{inter}} \rangle$ values, and fully elongated β -sheet strands. Each β -sheet monomer in the complex

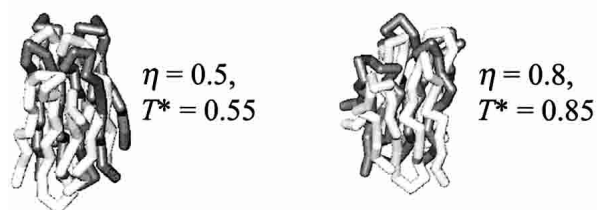
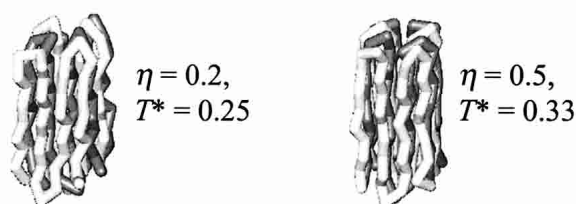
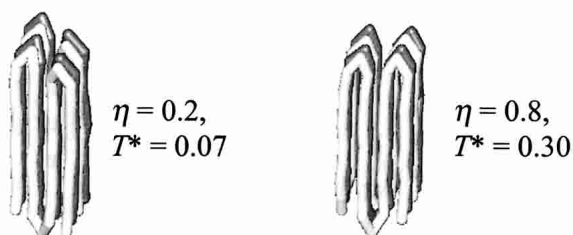
A Partially ordered β -sheet complex**B** Ordered β -sheet complex**C** Highly ordered β -sheet complex

Figure 10. Snapshots showing typical structures observed for the β -sheet complex in the final state. (A) The partially ordered β -sheet complex for $\eta = 0.5$ at $T^* = 0.55$ and for $\eta = 0.8$ at $T^* = 0.85$. (B) The ordered β -sheet complex for $\eta = 0.2$ at $T^* = 0.25$ and for $\eta = 0.5$ at $T^* = 0.33$. (C) The highly ordered β -sheet complex for $\eta = 0.2$ at $T^* = 0.07$ and for $\eta = 0.8$ at $T^* = 0.30$.

structure displays the intrinsically long molecular shape found in the global energy minimum structure in Figure 1. The highly ordered β -sheet complex is in a solid-like phase and is tightly packed, preventing bead fluctuations and squeezing the β -sheets together. It is observed for all η at low temperatures.

The results for the β -sheet complex that we have just described are summarized in Figure 11, which shows the phases that occur in the space spanned by the reduced temperature T^* and the intermolecular contact parameter η . It can be seen from the phase diagram that there are four monomer states and three oligomer states. Starting at high temperatures, the four monomer states are four random coils, four disordered globules, four ordered globules, and four native β -sheet states. The three dotted lines in Figure 11 separating the four different monomer phases were ob-

tained from our previous thermodynamic study for isolated chain systems (Jang et al. 2002a). The monomer and oligomer states are separated by the line connecting solid circles. This boundary was obtained from the location of the temperature above which $\langle Q_{\text{inter}} \rangle = 0$. Slightly below this line is a narrow region in which various types of intermediates are observed. These intermediates are similar to the kinetic intermediates, I_{2+1+1} , I_{2+2} , and I_{3+1} that were observed in the kinetic study of the same model (Jang et al. 2003). The intermediates emerge when the systems start to dissociate as the temperature is raised, that is, when $\langle Q_{\text{inter}} \rangle$ decreases rapidly and $\langle R_g^2/\sigma^2 M \rangle$ increases abruptly. The line connecting the open triangles is associated with the emergence of the intermediates. The intermediates only exist over a very narrow temperature range and disappear when $\langle Q_{\text{inter}} \rangle = 0$. The system dissociation transition is located between the solid circle and open triangle lines. Below the system dissociation transition, there are three distinct oligomer phases for the β -sheet complex. The partially ordered β -sheet complex is observed at intermediate to large η at high temperatures, but is not observed for $\eta < 0.4$. As T^* decreases, the partially ordered β -sheet complex for $0.4 < \eta < 0.8$ has a subtle conformational change to the ordered β -sheet complex, whereas for $\eta > 0.8$ it changes directly to the highly ordered β -sheet complex, a solid-like phase. The transition from the partially ordered to the ordered β -sheet complex is determined from the small peak in the specific heat curve, whereas the transition to the highly ordered β -sheet complex is obtained from the low temperature peak in the specific heat curve and the Lindemann disorder parameter. The ordered β -sheet complex is observed at small to intermediate η at low temperatures, but is not observed for $\eta > 0.8$.

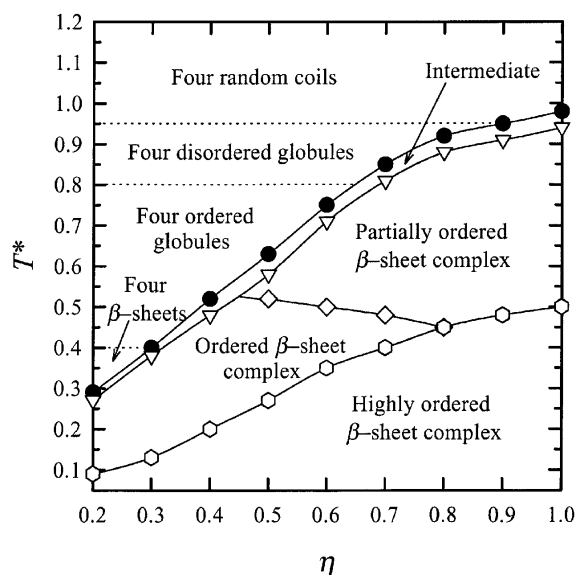


Figure 11. Phase diagram for the β -sheet complex as a function of the reduced temperature, T^* , and the intermolecular contact parameter, η .

As T^* decreases, the ordered β -sheet complex changes to the highly ordered β -sheet complex. For small η , the transition to the highly ordered β -sheet complex is determined from the Lindemann disorder parameter, whereas for intermediate η it is obtained from both the low temperature peak in the specific heat curve and the Lindemann disorder parameter. The highly ordered β -sheet complex exists at even lower temperatures for small η and at relatively high temperatures for large η . Regardless of the size of η and temperature, the highly ordered β -sheet complex is solid-like and has fully stiff β -sheet strands, the same as the global energy minimum structure.

Discussion

We have studied the thermodynamics and stability of a β -sheet complex that contains four identical four-stranded antiparallel β -sheet peptides. DMD simulations of the model complex have been performed for different sizes of the intermolecular contact parameter η , which measures the ratio of intermolecular to intramolecular native attractions, at a bias gap $g = 0.9$, a measure of the strength of the intramolecular native contacts relative to that of the intramolecular nonnative contacts.

The thermodynamic properties of the β -sheet complex strongly depend on the value of intermolecular contact parameter η and seem to be most representative of protein aggregation and fibril formation at intermediate values. Three distinct oligomer states are observed: the partially ordered β -sheet complex, the ordered β -sheet complex, and the highly ordered β -sheet complex. The partially ordered β -sheet complex is in a liquid-like phase and contains four ordered globules with $\langle Q_{\text{intra}} \rangle$ values in the range $0.5 < \langle Q_{\text{intra}} \rangle < 0.9$; the entire structure is not very tightly packed. It is more likely to exist at high η , assembles from four random coils, four disordered globules, or four ordered globules as T^* decreases, and is not observed at any temperature when $\eta < 0.4$. The ordered β -sheet complex is in a liquid-like phase, contains four native β -sheets with $\langle Q_{\text{intra}} \rangle > 0.90$, and is more tightly packed than the partially ordered β -sheet complex. The ordered β -sheet complex is more likely to exist as η decreases, assembles from four ordered globules or four native β -sheets as T^* decreases, and does not exist at $\eta > 0.8$. The highly ordered β -sheet complex is in a solid-like phase and is observed for all η at low temperatures. The highly ordered β -sheet complex contains four native β -sheets with highly stiff β -strands, which are assembled face to face forming a highly ordered structure, the same as the global energy minimum structure. The highly ordered β -sheet complex is formed from the partially ordered β -sheet complex at large η or from the ordered β -sheet complex at small η as T^* decreases. No direct conformational change from the monomer states to the highly ordered oligomer is observed.

There is a good deal of evidence based on experimental observations that protein aggregation, including amyloid fibril formation, arises directly from partially folded intermediates (Kelly 1996; Booth et al. 1997; Fink 1998; Guijarro et al. 1998; Chiti et al. 1999; Quintas et al. 1999; Khurana et al. 2001). In fact, these partially folded intermediates are experimentally observed to be molten globules (Booth et al. 1997; Khurana et al. 2001). This is consistent with our observations for the intermediate η models that the partially ordered β -sheet complex and the ordered β -sheet complex assemble from four ordered globules (molten globules). However, for very small η ($\eta \leq 0.3$) at low temperatures and for very large η ($\eta \geq 0.9$) at high temperatures, the ordered β -sheet complex and the partially ordered β -sheet complex assemble from four native β -sheets and four random coils, respectively. Protein aggregation starting directly from random coils has also been observed in a recent experimental study of the two state folders, U1A and C12 (Silow et al. 1999); such behavior has also been observed in a recent simulations study of protein aggregation (Dima and Thirumalai 2002), albeit at low protein concentration.

Recently, Dima and Thirumalai (2002) reported a phase diagram similar to Figure 11 for a generic two-state lattice model with side chains in temperature/concentration space, instead of in T^*/η space. They found that there are three distinct oligomer states in the ordered region in the phase diagram: amorphous, ordered, and glassy oligomers. The amorphous oligomers are observed at relatively high temperatures and high concentrations; the ordered oligomers are located at low temperatures and low concentrations; and the glassy oligomers are located at low temperatures and high concentrations. In analogy with our results, their amorphous, ordered, and glassy oligomers correspond to our partially ordered, ordered, and highly ordered β -sheet complexes, respectively. This indicates that the intermolecular contact parameter η can be used to mimic the effect of protein concentration.

Our coarse-grained off-lattice protein models interacting via Go-type potentials (Taketomi et al. 1975; Go and Taketomi 1978, 1979; Ueda et al. 1978) are very simple. Clearly, minimalist models based on Go-type potentials have limitations that prevent them from mimicking some aspects of the folding of real proteins. Our Go-model with the intermediate parameter value is similar to the contact-dominant C_α model of Kaya and Chan (2003) in two ways. First, as was the case for the isolated β -sheet protein model (Jang et al. 2002a), the β -sheet complex model is not calorimetrically cooperative (Kaya and Chan 2002). Second, it does not include local conformational stiffness, which would have made the model more protein-like. Our Go-model with the intermediate parameter value differs, however, from the contact-dominant model in that it exhibits a weak bimodal energy distribution in its disordered-to-ordered globule transition (Jang et al. 2002a), whereas the

contact-dominant model displays a single distribution. Kaya and Chan (2002) have pointed out that if the thermodynamics of a model do not satisfy the calorimetric two-state criterion, its folding kinetics is not likely to be protein-like. The implications of these limitations for the present work are unclear because the general mechanism governing protein aggregation is somewhat different from that governing protein folding and is certainly more complicated. Even with these limitations, Go-type protein models often yield a number of insights into the basic principles behind the thermodynamics and kinetics of protein folding and aggregation (Zhou and Karplus 1997a,b, 1999; Dokholyan et al. 1998, 2000; Bratko and Blanch 2001; Jang et al. 2002a,b).

Our model of a β -sheet complex could prove useful in understanding the basic principles behind A β fibril formation. However, it would have rendered more insights into fibril formation and stability if the native state of the monomer had been different from that in the aggregate, because the native conformation of a peptide in solution is usually different from that in aggregates. This is a limitation of the Go-type potential that we have devised. In fact, this deficiency might affect the kinetics of the β -sheet complex more than the thermodynamics. Many amyloid forming peptides, including A β peptides, are thought to be random coils in solution under most conditions but are extended chains or β -hairpins in fibrils (Serpell 2000). In an effort to remedy this deficiency, studies of fibril formation kinetics for a system of β -hairpins as a function of chain concentration are being conducted.

Acknowledgments

This work was supported by the NIH under grant GM-56766 and the NSF under grant CTS-9704044. The work at Buffalo is supported in part by a grant from HHMI to SUNY Buffalo.

The publication costs of this article were defrayed in part by payment of page charges. This article must therefore be hereby marked "advertisement" in accordance with 18 USC section 1734 solely to indicate this fact.

References

- Alder, B.J. and Wainwright, T.E. 1959. Studies in molecular dynamics, I: General method. *J. Chem. Phys.* **31**: 459–466.
- Benzinger, T.L.S., Gregory, D.M., Burkoth, T.S., Miller-Auer, H., Lynn, D.G., Botto, R.E., and Meredith, S.C. 1998. Propagating structure of Alzheimer's β -amyloid(10–35) is parallel β -sheet with residues in exact register. *Proc. Natl. Acad. Sci.* **95**: 13407–13412.
- . 2000. Two-dimensional structure of β -amyloid(10–35) fibrils. *Biochemistry* **39**: 3491–3499.
- Bilgram, J.H. 1987. Dynamics at solid liquid transition-experiments at the freezing-point. *Phys. Rep.* **153**: 1–89.
- Booth, D.R., Sunde, M., Bellotti, V., Robinson, C.V., Hutchinson, W.L., Fraser, P.E., Hawkins, P.N., Dobson, C.M., Radford, S.E., Blake, C.C.F., et al. 1997. Instability, unfolding and aggregation of human lysozyme variants underlying amyloid fibrillogenesis. *Nature* **385**: 787–793.
- Bratko, D. and Blanch, H.W. 2001. Competition between protein folding and aggregation: A three-dimensional lattice-model simulation. *J. Chem. Phys.* **114**: 561–569.
- Burkoth, T.S., Benzinger, T.L.S., Jones, D.N.M., Hallenga, K., Meredith, S.C., and Lynn, D.G. 1998. C-terminal PEG blocks the irreversible step in β -amyloid(10–35) fibrillogenesis. *J. Am. Chem. Soc.* **120**: 7655–7656.
- Chan, H.S. and Dill, K.A. 1994. Transition states and folding dynamics of proteins and heteropolymers. *J. Chem. Phys.* **100**: 9238–9257.
- Chiti, F., Webster, P., Taddei, N., Clark, A., Stefani, M., Ramponi, G., and Dobson, C.M. 1999. Designing conditions for in vitro formation of amyloid protofilaments and fibrils. *Proc. Natl. Acad. Sci.* **96**: 3590–3594.
- Clark, J. and Steele, J. 1992. Phase separation inhibitors and prevention of selenite cataract. *Proc. Natl. Acad. Sci.* **89**: 1720–1724.
- Dill, K.A. and Stigter, D. 1995. Modeling protein stability as heteropolymer collapse. *Adv. Protein Chem.* **46**: 59–104.
- Dima, R.I. and Thirumalai, D. 2002. Exploring protein aggregation and self-propagation using lattice models: Phase diagram and kinetics. *Protein Sci.* **11**: 1036–1049.
- Dokholyan, N.V., Buldyrev, S.V., Stanley, H.E., and Shakhnovich, E.I. 1998. Discrete molecular dynamics studies of the folding of a protein-like model. *Fold. Des.* **3**: 577–587.
- . 2000. Identifying the protein folding nucleus using molecular dynamics. *J. Mol. Biol.* **296**: 1183–1188.
- Eaton, W.A. and Hofrichter, J. 1990. Sick cell hemoglobin polymerization. *Adv. Protein Chem.* **40**: 63–279.
- Esler, W.P., Stimson, E.R., Ghilardi, J.R., Vinters, H.V., Lee, J.P., Mantyh, P.W., and Maggio, J.E. 1996. In vitro growth of Alzheimer's disease β -amyloid plaques displays first-order kinetics. *Biochemistry* **35**: 749–757.
- Esler, W.P., Felix, A.M., Stimson, E.R., Lachenmann, M.J., Ghilardi, J.R., Lu, Y., Vinters, H.V., Mantyh, P.W., Lee, J.P., and Maggio, J.E. 2000. Activation barriers to structural transition determine deposition rates of Alzheimer's disease A β amyloid. *J. Struct. Biol.* **130**: 174–183.
- Ferrenberg, A.M. and Swendsen, R.H. 1989. Optimized Monte Carlo data analysis. *Phys. Rev. Lett.* **63**: 1195–1197.
- Fink, A.L. 1998. Protein aggregation: Folding aggregates, inclusion bodies and amyloid. *Fold. Des.* **3**: R9–R23.
- Fraser, P.E., Duffy, L.K., O'Malley, M.B., Nguyen, J.T., Inouye, H., and Kirschner, D.A. 1991a. Morphology and antibody recognition of synthetic β -amyloid peptides. *J. Neurosci. Res.* **28**: 474–485.
- Fraser, P.E., Nguyen, J.T., Surewicz, W.K., and Kirschner, D.A. 1991b. pH-dependent structural transitions of Alzheimer amyloid peptides. *Biophys. J.* **60**: 1190–1201.
- Gallo, G., Goni, F., Boctor, F., Vidal, R., Kumar, A., Stevens, F.J., Frangione, B., and Ghiso, J. 1996. Light chain cardiomyopathy: Structural analysis of the light chain tissue deposits. *Am. J. Pathol.* **148**: 1397–1406.
- Go, N. and Taketomi, H. 1978. Respective roles of short range and long range interactions in protein folding. *Proc. Natl. Acad. Sci.* **75**: 559–563.
- . 1979. Studies on protein folding, unfolding and fluctuations by computer simulation, IV: Hydrophobic interactions. *Int. J. Protein Res.* **13**: 447–461.
- Guijarro, J.I., Sunde, M., Jones, J.A., Campbell, I.D., and Dobson, C.M. 1998. Amyloid fibril formation by an SH3 domain. *Proc. Natl. Acad. Sci.* **95**: 4224–4228.
- Guo, Z. and Brooks III, C.L. 1997. Thermodynamics of protein folding: A statistical mechanical study of a small all- β protein. *Biopolymers* **42**: 745–757.
- Guo, Z., and Thirumalai, D. 1995. Kinetics of protein folding: Nucleation mechanism, time scales, and pathways. *Biopolymers* **36**: 83–102.
- . 1996. Kinetics and thermodynamics of folding of a de novo designed four-helix bundle protein. *J. Mol. Biol.* **263**: 323–343.
- Gupta, P. and Hall, C.K. 1997. Effect of solvent conditions upon refolding pathways and intermediates for a simple lattice protein. *Biopolymers* **42**: 399–409.
- . 1998. Effect of denaturant and protein concentrations upon protein refolding and aggregation: A simple lattice model. *Protein Sci.* **7**: 2642–2652.
- Gupta, P., Hall, C.K., and Voegler, A. 1999. Computer simulation of the competition between folding and aggregation. *Fluid Phase Equilib.* **158**: 87–93.
- Harper, J.D., Wong, S.S., Lieber, C.M., and Lansbury Jr., P.T. 1997. Observation of metastable A β amyloid protofibrils by atomic force microscopy. *Chem. Biol.* **4**: 119–125.
- Harrison, P.M., Chan, H.S., Prusiner, S.B., and Cohen, F.E. 1999. Thermodynamics of model prions and its implications for the problem of prion protein folding. *J. Mol. Biol.* **286**: 593–606.
- . 2001. Conformational propagation with prion-like characteristics in a simple model of protein folding. *Protein Sci.* **10**: 819–835.
- Jang, H., Hall, C.K., and Zhou, Y. 2002a. Folding thermodynamics of model four-strand antiparallel β -sheet proteins. *Biophys. J.* **82**: 646–659.
- . 2002b. Protein folding pathways and kinetics: Molecular dynamics simulations β -strand motifs. *Biophys. J.* **83**: 819–835.

- . 2003. Assembly and kinetic folding pathways of a tetrameric-sheet complex: Molecular dynamics simulations on simplified off-lattice protein models. *Biophys. J.* (in press).
- Kaya, H. and Chan, H.S. 2002. Towards a consistent modeling of protein thermodynamic and kinetic cooperativity: How applicable is the transition state picture to folding and unfolding? *J. Mol. Biol.* **315**: 899–909.
- . 2003. Solvation effects and driving forces for protein thermodynamic and kinetic cooperativity: How adequate is native-centric topological modeling? *J. Mol. Biol.* **326**: 911–931.
- Kelly, J.W. 1996. Alternative conformations of amyloidogenic proteins govern their behavior. *Curr. Opin. Struct. Biol.* **6**: 11–17.
- Khurana, R., Gillespie, J.R., Talapatra, A., Minert, L.J., Ionescu-Zanetti, C., Millett, I., and Fink, A.L. 2001. Partially folded intermediates as critical precursors of light chain amyloid fibrils and amorphous aggregates. *Biochemistry* **40**: 3525–3535.
- Kirkitadze, M.D., Bitan, G., and Teplow, D.B. 2002. Paradigm shifts in Alzheimer's disease and other neurodegenerative disorders: The emerging role of oligomeric assemblies. *J. Neurosci. Res.* **69**: 567–577.
- Kolinski, A., Galazka, W., and Skolnick, J. 1995. Computer design of idealized β -motifs. *J. Chem. Phys.* **103**: 10286–10297.
- Kolinski, A., Ilkowsky, B., and Skolnick, J. 1999. Dynamics and thermodynamics of β -hairpin assembly: Insights from various simulation techniques. *Biophys. J.* **77**: 2942–2952.
- Kowalewski, T. and Holtzman, D.M. 1999. In situ atomic force microscopy study of Alzheimer's β -amyloid peptide on different substrates: New insights into mechanism of β -sheet formation. *Proc. Natl. Acad. Sci.* **96**: 3688–3693.
- Lau, K.F. and Dill, K.A. 1989. A lattice statistical mechanics model of the conformational and sequence spaces of protein. *Macromolecules* **22**: 3986–3997.
- Lazaridis, T. and Karplus, M. 1997. "New view" of protein folding reconciled with the old through multiple unfolding simulations. *Science* **278**: 1928–1931.
- Lazo, N.D. and Cawning, D.T. 1998. Amyloid fibrils may be assembled from β -helical protofibrils. *Biochemistry* **37**: 1731–1735.
- Lindemann, F.A. 1910. The calculation of molecular vibration frequencies. *Physik. Z.* **11**: 609–612.
- Löwen, H. 1994. Melting, freezing and colloidal suspensions. *Phys. Rep.* **237**: 249–324.
- Lynn, D.G. and Meredith, S.C. 2000. Review: Model peptides and the physicochemical approach to β -amyloids. *J. Struct. Biol.* **130**: 153–173.
- Massry, S. and Glasscock, R. 1983. *Textbook of nephrology*. Williams & Wilkins, Baltimore, MD.
- Miller, R., Danko, C.A., Fasolka, M.J., Balazs, A.C., Chan, H.S., and Dill, K.A. 1992. Folding kinetics of proteins and copolymers. *J. Chem. Phys.* **96**: 768–780.
- Moore, R.C. and Melton, D.W. 1997. Transgenic analysis of prion diseases. *Mol. Hum. Reprod.* **3**: 529–544.
- Nymeyer, H., Garcia, A.E., and Onuchic, J.N. 1998. Folding funnels and frustration in off-lattice minimalist protein landscapes. *Proc. Natl. Acad. Sci.* **95**: 5921–5928.
- Pace, C.N., Hebert, E.J., Shaw, K.L., Schell, D., Both, V., Krajcikova, D., Sevcik, J., Wilson, K.S., Dauter, Z., Hartley, R.W., et al. 1998. Conformational stability and thermodynamics of folding of ribonucleases Sa, Sa2 and Sa3. *J. Mol. Biol.* **279**: 271–286.
- Pallitto, M.M. and Murphy, R.M. 2001. A mathematical model of the kinetics of β -amyloid fibril growth from the denatured state. *Biophys. J.* **81**: 1805–1822.
- Pande, V.S. and Rokhsar, D.S. 1998. Is the molten globule a third phase of proteins? *Proc. Natl. Acad. Sci.* **95**: 1490–1494.
- Plaxco, K.W., Simons, K.T., and Baker, D. 1998. Contact order, transition state placement and the refolding rates of single domain proteins. *J. Mol. Biol.* **277**: 985–994.
- Ptitsyn, O.B. 1995. Molten globule and protein folding. *Adv. Protein Chem.* **47**: 83–230.
- Quintas, A., Saraiva, M.J.M., and Brito, R.M.M. 1999. The tetrameric protein transthyretin dissociates to a non-native monomer in solution: A novel model for amyloidogenesis. *J. Biol. Chem.* **274**: 32943–32949.
- Rapaport, D.C. 1978. Molecular dynamics simulation of polymer chains with excluded volume. *J. Phys. A Math. Gen.* **11**: L213–L216.
- Sali, A., Shakhnovich, E.I., and Karplus, M. 1994. Kinetics of protein folding: A lattice model study of the requirements for folding to the native state. *J. Mol. Biol.* **235**: 1614–1636.
- Selkoe, D.J. 1991. Alzheimer's disease: A central role for amyloid. *J. Neuro-path. Exp. Neurol.* **53**: 438–447.
- Serpell, L.C. 2000. Alzheimer's amyloid fibrils: Structure and assembly. *Biochim. Biophys. Acta* **1502**: 16–30.
- Shea, J.-E., Onuchic, J.N., and Brooks III, C.L. 2000. Energetic frustration and the nature of the transition state in protein folding. *J. Chem. Phys.* **113**: 7663–7671.
- Silow, M., Tan, Y.J., Fersht, A.R., and Oliveberg, M. 1999. Formation of short-lived protein aggregates directly from coil in two-state folding. *Biochemistry* **38**: 13006–13012.
- Simmons, L.K., May, P.C., Tomoselli, K.J., Rydel, R.E., Fuson, K.S., Brigham, B.F., Wright, S., Lieberburg, I., Becker, G.W., Brems, D.N., et al. 1994. Secondary structure of amyloid β peptide correlates with neurotoxic activity in vitro. *Mol. Pharmacol.* **45**: 373–379.
- Skolnick, J. and Kolinski, A. 1991. Dynamic Monte Carlo simulations of a new lattice model of globular protein folding, structure and dynamics. *J. Mol. Biol.* **221**: 499–531.
- Smith, S.W., Hall, C.K., and Freeman, B.D. 1996. Molecular dynamic study of entangled hard-chain fluids. *J. Chem. Phys.* **104**: 5616–5637.
- Snyder, S.W., Lador, U.S., Wade, W.S., Wang, G.T., Barrett, L.W., Matayoshi, E.D., Huffaker, H.J., Krafft, G.A., and Holzman, T.F. 1994. Amyloid- β aggregation: Selective inhibition of aggregation in mixtures of amyloid with different chain lengths. *Biophys. J.* **67**: 1216–1228.
- Stillinger, F.H. 1995. A topographic view of super-cooled liquids and glass formation. *Science* **267**: 1935–1939.
- Sunde, M., Serpell, L.C., Bartlam, M., Fraser, P.E., Pepys, M.B., and Blake, C.C.F. 1997. Common core structure of amyloid fibrils by synchrotron X-ray diffraction. *J. Mol. Biol.* **273**: 729–739.
- Taketomi, H., Ueda, Y., and Go, N. 1975. Studies on protein folding, unfolding and fluctuations by computer simulation: The effect of specific amino acid sequence represented by specific inter-unit interactions. *Int. J. Pept. Protein Res.* **7**: 445–459.
- Ueda, Y., Taketomi, H., and Go, N. 1978. Studies on protein folding, unfolding and fluctuations by computer simulation, II: A three-dimensional lattice model of lysozyme. *Biopolymers* **17**: 1531–1548.
- Zhang, S., Iwata, K., Lachenmann, M.J., Peng, J.W., Li, S., Stimson, E.R., Lu, Y., Felix, A.M., Maggio, J.E., and Lee, J.P. 2000. The Alzheimer's peptide A β adopts a collapsed coil structure in water. *J. Struct. Biol.* **130**: 130–141.
- Zhou, Y. and Karplus, M. 1997a. Folding thermodynamics of a model three-helix bundle protein. *Proc. Natl. Acad. Sci.* **94**: 14429–14432.
- . 1997b. Interpreting the folding kinetics of helical proteins. *Nature* **401**: 400–403.
- . 1999. Folding of a model three-helix bundle protein: A thermodynamic and kinetic analysis. *J. Mol. Biol.* **293**: 917–951.
- Zhou, Y., Hall, C.K., and Karplus, M. 1996. First-order disorder-to-order transition in an isolated homopolymer model. *Phys. Rev. Lett.* **77**: 2822–2825.
- Zhou, Y., Karplus, M., Wichert, J.M., and Hall, C.K. 1997. Equilibrium thermodynamics of homopolymers and clusters: Molecular dynamics and Monte Carlo simulations of systems with square-well interactions. *J. Chem. Phys.* **107**: 10691–10708.
- Zhou, Y., Vitkup, D., and Karplus, M. 1999. Native proteins are surface-molten solids: Application of the Lindemann criterion for the solid versus liquid state. *J. Mol. Biol.* **285**: 1371–1375.